Supporting Online Material for

20th-Century Industrial Black Carbon Emissions Altered Arctic Climate Forcing

Joseph R. McConnell,* Ross Edwards, Gregory L. Kok, Mark G. Flanner, Charles S. Zender, Eric S. Saltzman, J. Ryan Banta, Daniel R. Pasteris, Megan M. Carter, Jonathan D. W. Kahl

*To whom correspondence should be addressed. E-mail: Joe.McConnell@dri.edu

Published 9 August 2007 on *Science* Express
DOI: 10.1126/science.1144856

This PDF file includes:

Supporting Online Material

Materials and methods

Ice core collection and analysis

Two ice cores, identified as D4 and D5, were collected in 2003 from high snowfall regions of the west-central Greenland ice sheet (Fig. S1). Located at high elevation (2713 m above sea level) where summer surface melting is rare, the more northern D4 core (71.4^{o}N, 44.0^{o}W) was drilled to a depth of 144 m (*S1*). Located ~350 km to the south, the 150 m D5 core (68.5^{o}N, 42.9^{o}W) was drilled at a lower elevation (2473 m above sea level) where summer surface melting is common. Both cores were drilled with a 10 cm diameter electromechanical drill. The ~1 m long core sections were measured and weighed in the field and returned frozen to the National Ice Core Laboratory for sampling. Five parallel longitudinal samples were cut from the cores, each with a cross-section of ~3.5 by ~3.5 cm, and the samples were shipped frozen to our ultra-trace chemistry laboratory in Reno for analysis.

The D4 and D5 ice cores first were analyzed for a broad range of elements and chemical species using a unique continuous flow analysis system (*S2 –S4*). This system includes a traditional continuous flow analysis stage, two high resolution inductively coupled plasma mass spectrometers, and an inductively coupled plasma optical emission spectrometer. Analytes in this study included indicators of continental dust (aluminum, magnesium, calcium, iron), sea salts (sodium, magnesium, calcium, sulfur), industrial pollution (lead, sulfur, nitrate), explosive volcanism (sulfur), and atmospheric photochemistry (hydrogen peroxide). Nearly all analytes showed a strong seasonal cycle

that can be used for annual-layer counting. Although seasonal cycles for a number of analytes were used to confirm annual-layer identification, here we used minima in hydrogen peroxide concentration to identify the mid-winter horizon (nominally January 1 of each year) (*S5*). While hydrogen peroxide is frequently used for ice core dating in shallow cores, diffusion smoothes the annual cycle with time. At the D4 core site, high snowfall rates and cold temperatures mean that very distinct annual cycles in hydrogen peroxide are preserved throughout the cores, providing a means to obtain consistent sub-seasonal dating throughout the record (Fig. S2). While more diffused and disrupted by melt layers, accurate annual dating at the D5 site was accomplished using annual cycles in hydrogen peroxide, sulfur, and dust tracers such as aluminum and calcium. While BC measurements were made only over selected sections of the D5 ice core, comparison of the 95 annual average concentrations common to both the D4 and D5 records shows that changes in BC concentration during the past two centuries were coherent over large areas (Fig. S3).

For first analysis of the D4 ice core, we added a ThermoFinnigan Quantum electrospray-triple quadrupole mass spectrometer to the continuous flow analysis system, making possible high depth resolution, very low concentration measurements of polar organic and other molecules that are exactly co-registered with all other elemental and chemical measurements. As an indicator of fallout from biomass burning emissions, we measured vanillic acid (VA). Unlike ice core tracers of biomass burning such as ammonium ion (NH_4^+) or nitrate (NO_3^-) which have significant sources other than wildfires (*S6 – S8*), VA is predominantly emitted during biomass burning. VA emissions

are derived from combustion of lignin with coniferyl alcohol precursors. It is primarily associated with conifers, although it is also observed in minor amounts from combustion of deciduous trees and grasses (*S9 –S11*). VA was analyzed by diluting the ice core melt stream with methanol (50:50). Detection was done in the negative ion spectrum, using a mass transition of 167→123 to detect the parent $C_8H_7O_4^-$ ion and its collision product, $C_7H_7O_{12}^-$.

For a second analysis of the D4 ice core, we added a BC analyzer (SP2, Droplet Measurement Technologies, Boulder, Colorado) to the continuous flow analysis system to yield high depth resolution, very low concentration and size distribution measurements of BC in ice cores during recent centuries. Individual BC particles are counted in the method, and the counts accumulated during 30-second measurement intervals to derive BC particle number and mass distribution. The D4 ice core record contains an average of 13, 30-second measurement intervals per year from 1788 through 2002, with BC measurements exactly co-registered with all other elemental and chemical measurements. BC detection limits in the continuous ice core analysis are ~0.02 ng g^{-1}.

The SP2 uses a patented technique (*S12*) that measures mass of individual BC particles using laser-induced incandescence (see [*S13*] for additional details). BC particles pass through the laser beam intra-cavity of a diode-pumped Nd YAG laser (1.06 μm wavelength) where they absorb light. Circulating power in the cavity is in excess of 1 MW cm^{-2}. BC particles absorb sufficient energy as they pass through the laser beam and reach a temperature at which they incandesce. Intensity of the incandescence is measured with a photomultiplier tube and recorded. Mass of individual BC particles is proportional

to the area of the incandescence signal. The SP2 was calibrated using glassy carbon particles of known density with particle size selected using an electrostatic classifier. In this study, calibration was conducted over a particle mass range from 0.23 to 41 femtograms for individual particles.

Air Mass Back-Trajectory Modeling

To identify likely source regions for BC, VA, S, and other chemical and elemental tracers measured in the ice cores, we used the National Oceanographic and Atmospheric Administration (NOAA) three-dimensional atmospheric trajectory model (*S14*). Atmospheric velocity fields (1958 through 2002) from the ERA-40 reanalysis (*S15*) were used to drive the model. Previous work on continental dust in Greenland ice suggests that insoluble dust particles are transported from Asia over many days (*S16*). Three-day trajectories were used here, however, because modeling (*S17*) suggests conversion in the atmosphere of hydrophobic to hydrophilic BC in ~1.5 days from which we estimate an atmospheric lifetime of ~three days. The 12-hourly trajectories were analyzed using the three-dimensional residence time analysis methodology described by (*S18*).

Black Carbon Relative to Sulfur Dioxide Emissions and Non-Sea-Salt Sulfur

Examination of the D4 ice core records of BC and non-sea-salt sulfur (nss-S) provides a means to estimate net relative emissions between sulfur dioxide (SO_2) and BC. By net, we mean the bulk relationship between nss-S from many sources of SO_2 emissions and BC in Greenland precipitation after any modifications during transport. We used a 15-year sliding window from 1850 to 2002 to evaluate slope and significance of the correlation between BC and nss-S during winter when forest-fire-derived BC was at a minimum. Considering only 15-year periods when the correlation was significant ($p<0.05$), the mean slope of the linear regression was ~0.3, meaning that for every ton of pollution nss-S deposited in winter precipitation, 0.3 tons of BC were deposited concurrently. Net relative deposition ranged from ~0.03 to ~0.57, with values increasing sharply in ~1880, reaching a broad high in the early 20th century, followed by sharp declines in ~1920, ~1940, and again in 1951. Changes in fuel types in the U.S., Canada, and Europe (*S19*) rather than technological changes resulted in very low BC concentrations relative to nss-S during the second half of the 20th century when net relative deposition ranged from ~0.03 to ~0.09.

The portion of BC from biomass burning emissions was estimated for the period 1788 to 2002 from a linear regression between BC and VA prior to industrialization and then extrapolated to the full record using the VA concentrations. Industrial BC emissions were determined by subtracting the estimated biomass burning BC from the total. Implicit is the assumption that the ratio of BC to VA from biomass burning emissions is consistent

throughout the 215-year period. Large-scale changes in tree species in the boreal forest (e.g., the abundance of deciduous relative to conifer trees) could alter this ratio.

Radiative Transfer Modeling

BC surface radiative forcing calculations were conducted with the Snow, Ice, and Aerosol Radiative (SNICAR) model (*S17*). Following (*S20*) and (*S21*), hemispheric radiative fluxes are derived in SNICAR from Mie ice and aerosol optical properties using a multi-layer solution and delta-hemispheric mean approximation for multiple scattering (*S22*). We estimated surface incident solar radiative fluxes for the ice core site using the Shortwave NarrowBand (SWNB) radiative transfer model (*S23*), applying typical sub-Arctic summer clear-sky and cloudy atmospheric profiles.

Because the D4 ice core site is located at high elevation in a region of little or no summer melting, we assumed an ice grain effective radius of 100 μm. Snow aerosol radiative forcing increases with increasing grain size so our grain size choice contributes to a conservative forcing estimate. For BC optical properties, we used the mean of the measured median particle masses (1.82 femtograms) and geometric lognormal distribution (2.64) as well as BC indices of refraction from (*S24*) and a particle density of 1250 kg m^{-3}. In addition, we assumed that BC particles deposited in Greenland snow are sulfate-coated with a shell radius 1.33 times greater than the BC core, which is consistent with an industrial source. Together, these assumptions produce a BC mass absorption cross-section (MAC) of 8.5m^2 g^{-1}at 550 nm, greater than the recommended MAC of 7.5

m^2 g^{-1} for freshly-combusted BC (*S25*) but smaller than that of thickly-coated particles whose MAC can be amplified by a factor of 1.5 (*S26*).

We generated a high-resolution lookup table of spectrally-resolved (470 band) albedo perturbation from varying amounts of BC and zenith angle for clear and cloudy skies. Using this table, we then estimated clear- and cloudy-sky radiative forcing at half-hour resolution for the full 1788 to 2002 time series, using zenith angle computed from (*S27*). While clear- and cloudy-sky time series bound plausible forcing variability from sky conditions, there is surprisingly little reduction (~10%) in surface forcing under thickly-clouded skies over Greenland. This insensitivity occurs because (1) more of the insolation reduction caused by clouds is in the near-infrared, whereas the effect of BC on snow albedo is almost entirely in the visible; and (2) diffuse radiation has an effective zenith angle that is smaller than typical Greenland clear-sky conditions. Lowering the effective zenith angle increases forcing because radiation penetrates deeper into the snowpack. A monthly linear interpolation between clear sky and cloudy solar surface insolation from SWNB was derived to match that from reanalysis data at this location (*S28*). This weighting was applied to derive the all-sky forcing that we report (Fig. S4). The largest source of uncertainty in our forcing estimates is from BC optical properties.

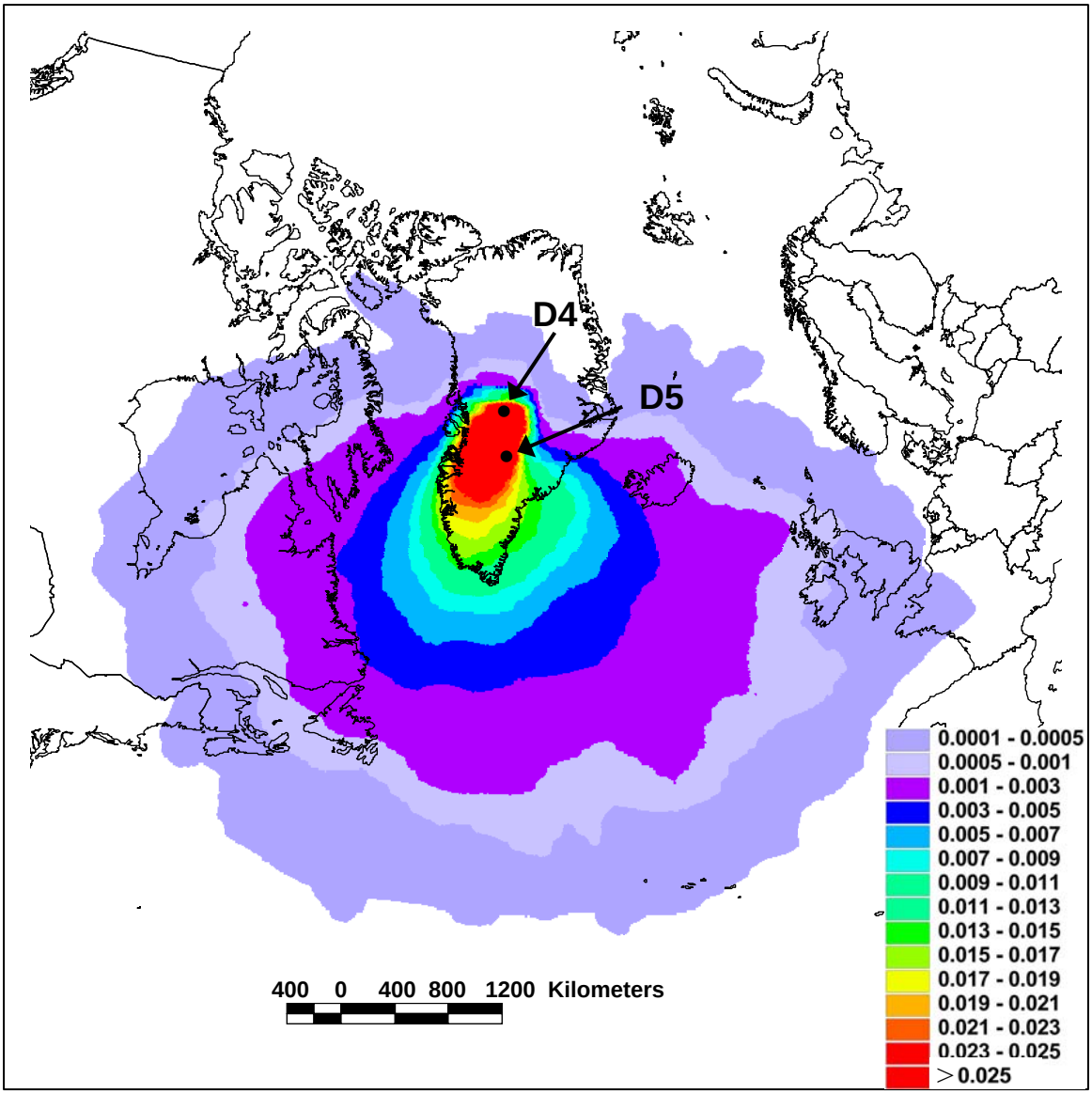

Fig. S1. Map of the Greenland region showing locations of the D4 and D5 ice cores. Also shown is the dimensionless air mass residence time for the D4 site based on three-day, three-dimensional back-trajectory modeling for the period from 1958 through 2002 using only trajectories corresponding to periods of significant snow accumulation at the core site as determined from the ERA-40 reanalysis (*S15*). Dimensionless total column residence times show the cumulative time (normalized to 1.0) that air mass trajectories arriving at the D4 ice core site passed over the indicated locations at altitudes of 0 to 1500 m.

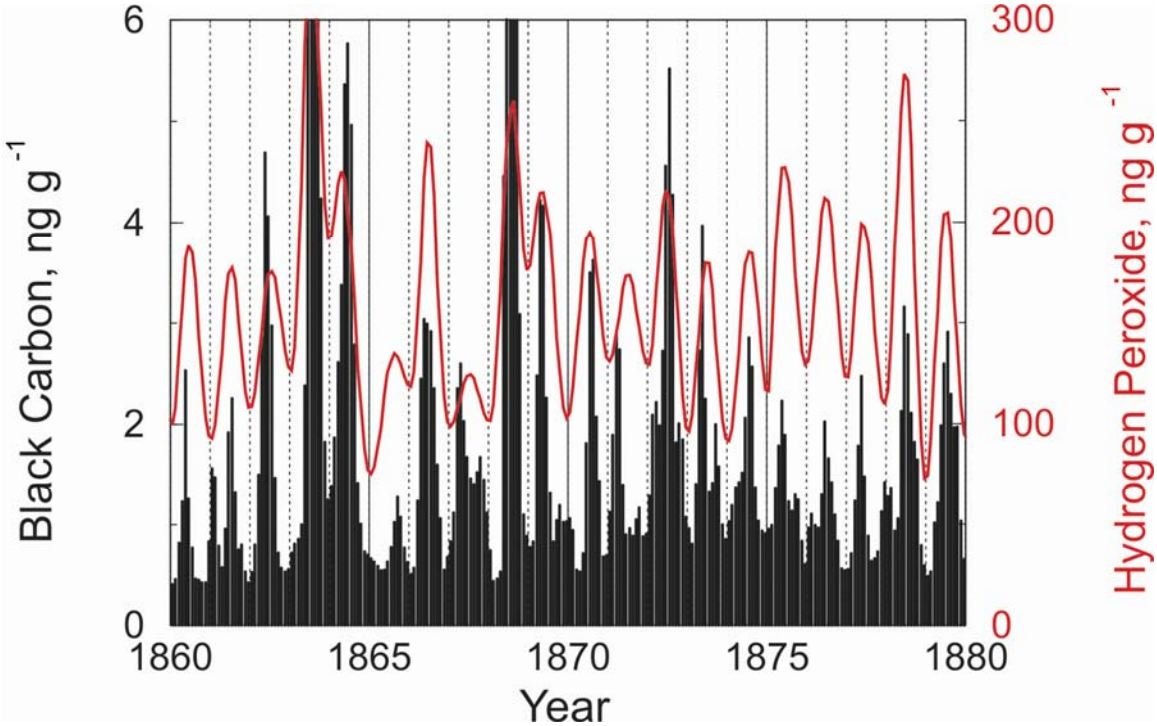

Fig. S2. Monthly averaged BC and hydrogen peroxide (H_2O_2) concentrations in the D4 ice core record from 1860 to 1880. The well preserved, strongly seasonal H_2O_2 record, together with a range of other elements and chemical species, were used to derive the depth-age relationship for the ice core. Note that BC concentrations generally peak in summer to early autumn coincident with the boreal forest fire season.

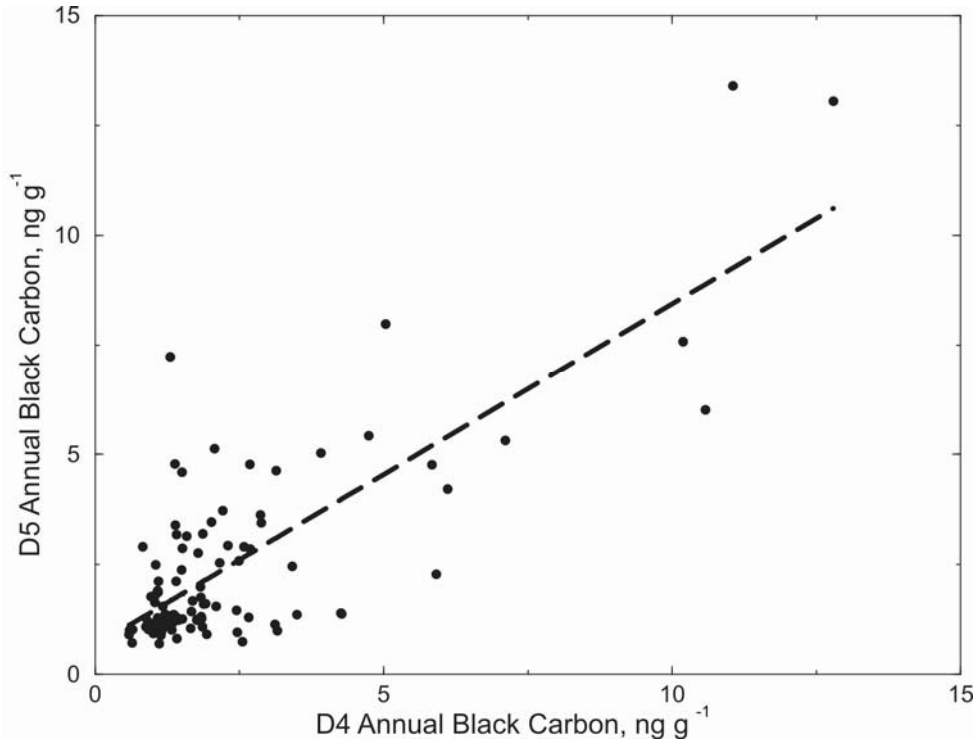

Fig. S3. Comparison of the 95 annual average BC concentrations measured in both the D4 and D5 ice cores during the period 1788 to 2002. The correlation (Pearson's R) is 0.77 ($p<0.0001$).

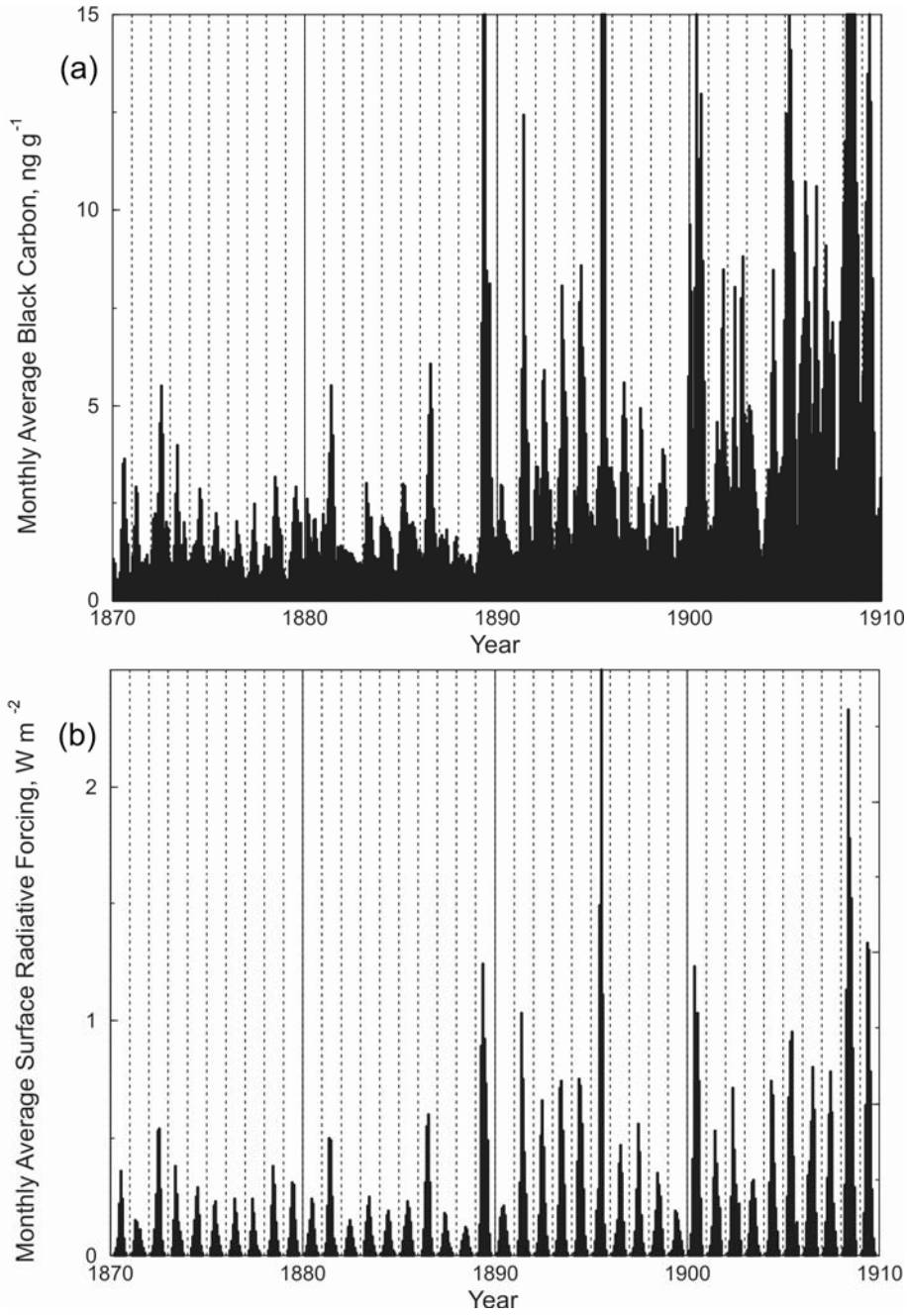

Fig. S4. Monthly BC concentration measured in the D4 ice core (a) and monthly averaged surface radiative forcing during the period from 1870 to 1910.

Supplementary references and notes

S1. J. R. Banta, J.R. McConnell, *J. Geophys. Res.,* **112**, 10.1029/2006JD007887 (2007).

S2. J. R. McConnell, G.W. Lamorey, S.W. Lambert, K.C. Taylor *Environ. Sci. Technol.* **36**, 7 (2002).

S3. J. R. McConnell, G. W. Lamorey, M. A. Hutterli, *Geophys. Res. Lett.,***29** (2002).

S4. J. R. McConnell, A.J. Aristarain, J.R. Banta, P.R. Edwards, J.C. Simões, *Proc. Natl. Acad. Sci.U.S.A.* **104**, 5732 (2007).

S5. J. R. McConnell, R. C. Bales, J. R. Winterle, H. Kuhns, C. R. Stearns, *J. Geophys. Res.,* **102**, 26809 (1997).

S6. G. Holdsworth *et al.*, *J. Geophys. Res.,* **101**, 23317 (1996).

S7. J.E. Dibb et al., *Atmos. Environ.,* **30**, 553 (1996).

S8. J. Savarino, M. Legrand, *J. Geophys. Res.,* **103**, 8267 (1998).

S9. D.R. Oros, B.R.T. Simoneit, *Appl. Geochem.*, **16**, 1545 (2001).

S10. D.R. Oros, B.R.T. Simoneit, *Appl. Geochem.*, **16**, 1513 (2001).

S11 D.R. Oros, M.R. bin Abas, J.Y.M.J. Omar, N.A. Rahman, B.R.T. Simoneit, *Appl. Geochem.,* **21**, 919 (2006).

S12. M. Stephens, N. Turner, J. Sandberg, *Appl. Optics*, **42**, 3726 (2003).

S13. J.P. Schwarz et al., *J. Geophys. Res.,* **111**, 10.1029/2006JD007076 (2006).

S14. J. M. Harris, J. D. W. Kahl, *J. Geophys. Res.,* **99**, 25845 (1994).

S15. S. M. Uppala *et al.*, *Q. J. R. Meteorol. Soc.,* **131**, 2961 (2005).

S16. P. E. Biscaye et al., *J. Geophys. Res.,* **102**, 26765 (1997).

S17. M. G. Flanner, C. S. Zender, J. T. Randerson, P. J. Rasch, *J. Geophys. Res.,* **112**, 10.1029/2006JD008003 (2007).

S18. J.E.Miller, J.D.W. Kahl, F. Heller, J.M. Harris, *Ann. Glaciol*., **35**, 403 (2002).

S19. T. Novakov *et al.*, *Geophys. Res. Lett.,* **30,** 10.1029/2002GL016345 (2003).

S20. W. J. Wiscombe, S. G. Warren (1980), *J. Atmos. Sci.*, **37**, 2712 (1980).

S21. S. Warren, W. Wiscombe, *J. Atmos. Sci.*, **37**, 2734 (1980).

S22. O. B. Toon, C. P. McKay, T. P. Ackerman, K. Santhanam *J. Geophys. Res.*, **94**, 16,287 (1989).

S23. C. S. Zender et al., *J. Geophys. Res.*, **102**, 29,901 (1997).

S24. H. Chang,, T. T. Charalampopoulos, *Proc. R. Soc. London Ser. A.*, **430**, 577 (1990).

S25. T.C. Bond, R. W. Bergstrom, *Aerosol Sci. Technol.*, **40**, doi:10.1080/02786820500421521 (2006).

S26. T.C. Bond, G. Habib, R. W. Bergstrom, *J. Geophys. Res.*, **111**, doi:10.1029/2006JD00731 (2006).

S27. A. Berger, *J. Atmos. Sci.*, **35**, 2362 (1978).

S28. T. Qian, A. Dai, K. E. Trenberth, K. W. Oleson, *J. Hydrometeorology*, **7**, 953 (2006).